The Application of Linear and Non-linear Two-Equation Turbulence Models in Hypersonic Flows

DOI:
10.2514/1.J061077

Document Version
Accepted author manuscript

The Application of Linear and Non-linear Two-Equation Turbulence Models in Hypersonic Flows

Haoyuan Zhang[1]
State Key Laboratory of Aerodynamics
Mianyang, 621000, People's Republic of China

China Aerodynamics Research and Development Center,
Mianyang, 621000, People's Republic of China

Thermo-Fluids Group, University of Manchester, Manchester, M13 9PL, United Kingdom

and
Timothy Craft[2] and Hector Iacovides[3]
Thermo-Fluids Group, University of Manchester, Manchester, M13 9PL, United Kingdom

A non-linear two-equation *k-ε* model has been implemented in the OpenFOAM framework and has been assessed for the computation of hypersonic flows with shock boundary layer interactions (SWBLI), together with two other linear, low-Reynolds number models, namely the Launder-Sharma *k-ε* model and the *k-ω* SST model. Supersonic and hypersonic flow computations resulting from the use of these three models have been compared with experimental benchmark cases over a range of conditions. The three original models tested do generally return reasonable predictions of wall pressure in most cases, with the non-linear model resulting in the best capability among the three in predicting flow separation. The wall heat flux in the interaction region, however, is overpredicted, in most cases by all three models (sometimes showing quite a dramatic overprediction). While the overall wall heat flux predictions of the non-linear model, are closer to the measured values, it is nevertheless evident that there is a need for further improvement. To address this need, the inclusion of a new source term in the dissipation rate equation is proposed, which aims to restrict the turbulent length scales in the shock wave boundary layer interaction region. This is inactive

[1] Associate Research Professor, Computational Aerodynamics Institute; haoyuan.zhang@cardc.cn (corresponding author)
[2] Senior Lecturer, Thermo-Fluids Group, Department of Mechanical, Aerospace & Civil Engineering
[3] Professor, Thermo-Fluids Group, Department of Mechanical, Aerospace & Civil Engineering

in incompressible flows and exerts only a minor influence in supersonic SWBLI cases. Computations of a range of supersonic and hypersonic flows with SWBLI show that this inclusion of the proposed source term in the dissipation rate equation, of both the non-linear and the linear *k*-ε models, has significant effects only in hypersonic flows. These effects are mainly confined to the thermal predictions of these *k*-ε models. In the non-linear model predictions, the over-estimation of the wall heat flux in the SWBLI region is largely eliminated, while in the corresponding predictions of the linear model the over-estimation is substantially reduced. The cubic non-linear *k*-ε model tested, with the proposed new source term to the dissipation rate equation, is thus shown to be a very reliable and cost-effective tool for the RANS modeling of supersonic and hypersonic flows.

Nomenclature

a_{ij} = Anisotropic stress tensor

C_f = Skin-friction coefficient, $(= \tau_w / \frac{1}{2}\rho_\infty U_\infty^2)$

k = Turbulent kinetic energy

l = Turbulent length scale

P_k = Production rate in the *k* transport equation

S = Strain invariant

δ = Boundary layer thickness

δ^* = Displacement thickness

θ = Momentum thickness

ε = Dissipation rate of turbulent kinetic energy

$\tilde{\varepsilon}$ = Isotropic Dissipation rate of turbulent kinetic energy

δ_{ij} = Kronecker's delta

ω = Specific dissipation rate of turbulent kinetic energy ($= \frac{\varepsilon}{k}$)

Subscripts

∞ = Freestream value

w = Value at the wall

0 = Value of the incoming boundary layer

I. Introduction

The interaction between a shock wave and the boundary layer at high-speed flights is ubiquitous, and might occur between many components and structures of aircrafts, rockets and space shuttles [1]. One important feature of shock wave boundary layer interaction is the flow separation caused by the adverse pressure gradient imposed in the neighbourhood of the boundary layer by shock waves, which might cause, for instance, a strong loss of total pressure in the inlet tunnel of a scramjet engine. Another typical feature is the compressibility effect (much stronger than that in the supersonic regime), which typically leads to strong amplification of local wall pressure and heat flux after the reattachment of boundary layer separation.

In the case of SWBLIs in hypersonic turbulent flows, many turbulence models have been examined, and their results compared to a variety of experimental measurements [2]. Two major defects have typically been reported in the predictions of such flows: one is the lack of accuracy in predicting flow separations induced by shock wave, and the other is the strong overprediction of wall heat flux in the interaction region. Some modifications, such as the turbulent length scale correction of Coakley [3] or compressibility corrections of Rubesin [4], and Vuong and Coakley [5] to improve the predictions of flows with SWBLIs, have been explored. These investigations were mainly confined within the context of linear EVMs, and some of them do help to overcome some weaknesses seen in certain models when predicting flow separation or wall heat flux. However, in many cases these methods have not been widely tested, and may cause other issues, such as having a negative impact on incompressible flows or leading to worse predictions of other “simple” flows that the original model did predict reasonably well [6, 7]. Furthermore, the studies of Huang et al. [8], and Duan et al. [9] on compressible turbulent boundary layer flows by the use of direct numerical simulation (DNS) suggest that the failure to correctly predict the wall heat flux in the interaction region may be due to the use of constant turbulent Prandtl number. Xiao et al. [10] proposed a linear eddy viscosity model (EVM) with the use of

variable turbulent Prandtl number, and the predicted peak of wall heat flux was reduced significantly. Recently, based on the data from scale-resolving simulation methods, Jordan et al. [11, 12] directed their efforts to the development of modifications to improve the performance of traditional turbulence models in the predictions of flow separation and wall heat flux in the regions with SWBLI, where the influence of variable turbulent Prandtl number and the estimations of turbulent length scale and turbulent production were considered.

Another way of potentially addressing some of the model defects noted above is to use more advanced turbulence models than the widely-employed linear EVMs. Reynolds stress transport models (RSTMs) can naturally account for more flow physics, such as Reynolds-stress anisotropy, streamline curvature and swirl effects, but require greater computational resources and, in complex applications, may show some weakness in numerical stability. Although forms of such models have been applied to certain classes of supersonic flows, few, if any, reported uses of them for hypersonic flows. A possible alternative is the use of non-linear two-equation models, a type of EVMs using a non-linear strain-stress relation, which can offer the potential of returning more realistic representation of the turbulence field than linear EVMs, but only requiring a moderate increase of computer resources. Progress in the use of such models in the predictions of challenging cases in low speed incompressible flows has been made [13].

Therefore, the objective of this study is to assess the ability of such non-linear EVMs in the prediction of SWBLIs in hypersonic flows, using experimental data over a range of Mach and Reynolds numbers. In this paper, the non-linear two-equation k-ε model of Craft et al. [13] (CLS model) is applied to the computations of four benchmark cases, one supersonic SWBLI case and three hypersonic ones. The cases considered involve impinging shock interaction, where the externally fixed shock wave position dictates the location of the shock wave boundary layer interactions, and compression corner flows, in which the resulting flow separation from the SWBLI itself affects the positioning of the shock wave and interaction. As a comparison, two widely used linear EVMs, namely the linear two-equation k-ε model of Launder and Sharma [14] with Yap [15] correction (LSY model) and the linear two-equation k-ω mode of Menter, Kuntz and Langtry [16] (SST model), are applied to the prediction of the hypersonic cases employed as well. Although the non-linear EVM is found to result in a number of improvements over the linear model predictions, the wall heat flux in the interaction region is still overpredicted, and a turbulent length scale correction term is proposed to improve this. Its effect is shown in both the non-linear model and the linear LSY forms.

II. Numerical Implementation

The open source CFD platform, OpenFOAM, has been used to carry out all the simulations. A new density-based compressible solver has been developed during the course of this investigation, based on the existing compressible solver, rhoCentralFoam. One of the main differences between the new solver and rhoCentralFoam is the formulation of the RANS equations employed. In the new solver, several terms involving the turbulent kinetic energy in the mean momentum and energy transport equations, which are often neglected in solvers, have been included. These terms arise as a result of eddy-viscosity formulation for the Reynolds stresses and, as shown in [17], while their contribution in low speed flows is negligible, that is not the case in hypersonic flows involving SWBLI.

The other main addition to the new solver is the numerical scheme used for the convection terms: the AUSMPW+ (advection upstream splitting method by pressure-based weight function) [18] flux splitting scheme is used in the new solver. The other terms are discretized in a similar way as those in the existing solver. In particular, the 2nd order central scheme is used for diffusion terms, and to maintain the solution bounded, the 2nd order Total Variation Diminishing (TVD) method with the Van-Albada [19] limiter is used for the cell face interpolations. Local time marching with the 1st order implicit Euler method is used to accelerate convergence to steady-state, and the local Courant number is set to be less than 5.0 for the purpose of retaining numerical stability. Further details of the new solver and its validation can be found in ref [20, 21].

III.Turbulence Models

The non-linear *k-ε* model employed here has been developed by Craft et al. [13, 22] with cubic strain-stress relation and low-Reynolds-number effects. The closure coefficients were optimized over a range of incompressible flows, including simple shear, impinging, curved and swirling flows. In this model, the cubic stress-strain relation is as follows:

$$
\begin{aligned}
a_{ij} \equiv \frac{\overline{u_i'' u_j''}}{k} - \frac{2}{3}\delta_{ij} & \\
&= -\left(\frac{\nu_t}{k}\right) S_{ij} + C_1 \frac{\nu_t}{\tilde{\varepsilon}}\left(S_{ik}S_{jk} - \frac{1}{3}S_{mk}S_{mk}\delta_{ij}\right) + C_2 \frac{\nu_t}{\tilde{\varepsilon}}\left(\Omega_{ik}S_{kj} + \Omega_{jk}S_{ki}\right) \\
&+ C_3 \frac{\nu_t}{\tilde{\varepsilon}}\left(\Omega_{ik}\Omega_{jk} - \frac{1}{3}\Omega_{lk}\Omega_{lk}\delta_{ij}\right) + C_4 \frac{\nu_t k}{\tilde{\varepsilon}^2}\left(\Omega_{ki}S_{lj} + S_{kj}\Omega_{li}\right)S_{kl} \\
&+ C_5 \frac{\nu_t k}{\tilde{\varepsilon}^2}\left(\Omega_{il}\Omega_{lm}S_{mj} + S_{il}\Omega_{lm}\Omega_{mj} - \frac{2}{3}S_{lm}\Omega_{mn}\Omega_{nl}\delta_{ij}\right) + C_6 \frac{\nu_t k}{\tilde{\varepsilon}^2} S_{ij}S_{kl}S_{kl} \\
&+ C_7 \frac{\nu_t k}{\tilde{\varepsilon}^2} S_{ij}\Omega_{kl}\Omega_{kl}
\end{aligned}
\tag{1}
$$

where the strain and vorticity tensors are defined by

$$S_{ij} = \left(\frac{\partial \tilde{u}_i}{\partial x_j} + \frac{\partial \tilde{u}_j}{\partial x_i}\right) - \frac{2}{3}\frac{\partial \tilde{u}_k}{\partial x_k}\delta_{ij}, \qquad \Omega_{ij} = \left(\frac{\partial \tilde{u}_i}{\partial x_j} - \frac{\partial \tilde{u}_j}{\partial x_i}\right) \tag{2}$$

The homogeneous dissipation rate $\tilde{\varepsilon}$ is defined as $\tilde{\varepsilon} = \varepsilon - 2\nu(\partial k^{1/2}/\partial x_j)^2$ and the model coefficients $C_1, C_2, \ldots, C_7$ are given below.

$$C_1 = -0.1, \qquad C_2 = 0.1, \qquad C_3 = 0.26 \tag{3}$$

$$C_4 = -10C_\mu^2, \qquad C_5 = 0, \qquad C_6 = -5C_\mu^2, \qquad C_7 = 5C_\mu^2 \tag{4}$$

The transport equations for turbulent kinetic energy and its homogeneous dissipation rate are taken as follows:

$$\frac{\partial \overline{\rho} k}{\partial t} + \tilde{u}_i \frac{\partial \overline{\rho} k}{\partial x_j} = P_k - \varepsilon + \frac{\partial}{\partial x_j}\left(\overline{\rho}(\nu + \frac{\nu_t}{\sigma_k})\frac{\partial k}{\partial x_j}\right) \tag{5}$$

$$\frac{\partial \overline{\rho} \tilde{\varepsilon}}{\partial t} + \tilde{u}_i \frac{\partial \overline{\rho} \tilde{\varepsilon}}{\partial x_j} = C_{\varepsilon 1} f_1 \frac{\tilde{\varepsilon}}{k} P_k - C_{\varepsilon 2} f_2 \overline{\rho} \frac{\tilde{\varepsilon}^2}{k} + \frac{\partial}{\partial x_j}\left(\overline{\rho}\left(\nu + \frac{\nu_t}{\sigma_\varepsilon}\right)\frac{\partial \tilde{\varepsilon}}{\partial x_j}\right) + E + Y_c \tag{6}$$

where

$$P_k = -\overline{\rho u_i'' u_j''}\frac{\partial \tilde{u}_i}{\partial x_j} \tag{7}$$

Y_c is the length-scale correction term of Yap [15], which can be written:

$$Y_c = 0.83\frac{\tilde{\varepsilon}^2}{k}\max[\left(\frac{l}{l_e} - 1\right)\left(\frac{l}{l_e}\right)^2, 0] \tag{8}$$

where $l = k^{\frac{3}{2}}/\tilde{\varepsilon}$,$l_e = 2.5y$ and y is the distance to the nearest wall. The near-wall source term E is modelled as:

$$E = \begin{cases} 0.0022\dfrac{\nu_t \tilde{S} k^2}{\tilde{\varepsilon}}\left(\dfrac{\partial^2 \tilde{u}_i}{\partial x_j \partial x_k}\right)^2, & \text{for } \tilde{R}_t \leq 250, \\ 0, & \text{for } \tilde{R}_t \geq 250. \end{cases} \tag{9}$$

where the turbulence Reynolds number $\tilde{R}_t = k^2/\nu\tilde{\varepsilon}$.

The turbulent viscosity is modelled as

$$\nu_t = C_\mu f_\mu k^2/\tilde{\varepsilon} \tag{10}$$

where C_μ is a function of the strain and vorticity invariants $\tilde{S}$ and $\widetilde{\Omega}$:

$$C_\mu = \min\left[0.09, \frac{1.2}{1 + 3.5\eta + f_{RS}}\right] \tag{11}$$

with

$$\eta = \max\left(\tilde{S}, \widetilde{\Omega}\right)$$
$$\tilde{S} = \frac{k}{\tilde{\varepsilon}}\sqrt{\frac{1}{2}S_{ij}S_{ij}}, \qquad \widetilde{\Omega} = \frac{k}{\tilde{\varepsilon}}\sqrt{\frac{1}{2}\Omega_{ij}\Omega_{ij}} \tag{12}$$

and

$$f_{RS} = 0.235(\max(0, \eta - 3.333))^2 \exp\left(-\tilde{R}_t/400 + \sqrt{S_I^2}\right) \tag{13}$$

where $S_I = S_{ij}S_{jk}S_{ki}/(S_{nl}S_{nl}/2)^{3/2}$ is the non-dimensional form of the third invariant of the strain rate tensor.

The damping function f_μ is taken as

$$f_\mu = 1 - \exp\left(-(\tilde{R}_t/90)^{1/2} - (\tilde{R}_t/400)^2\right) \tag{14}$$

The closure coefficients and auxiliary relations are as follows:

$$C_{\varepsilon 1} = 1.44, \qquad C_{\varepsilon 2} = 1.92, \qquad \sigma_k = 1.0, \qquad \sigma_\varepsilon = 1.3 \tag{15}$$

$$f_1 = 1, \qquad f_2 = 1 - 0.3e^{-R_t^2} \tag{16}$$

IV. Results and Model Development

A. Performance of the Original Models

The first case used to examine the performance of the non-linear CLS model, as well as the two linear EVMs, is that investigated through the experiments of Kussoy and Horstman (1989) at a Mach number of 7.05. The test model of the experiment is shown in Fig. 1, for which flare angles of 20° and 35° are considered, with the former angle representing a fully attached flow and the latter one representing a fully separated one. The nominal freestream conditions are given in Table 1. The computations have been performed using a structured grid (see Fig. 2), uniform in the streamwise direction and expanding exponentially in the wall normal direction. The lengths of cylinder and flare are both set to be 20cm, which are long enough to cover the whole interaction region. The inlet boundary

condition has been obtained by first calculating an undisturbed cylinder boundary layer flow and matching the measured and computed displacement thickness at 6cm ahead of the corner. The no-slip condition was applied to the wall, with the wall temperature fixed to the experimental value and zero gradient for pressure. Zero-gradient conditions were applied for all variables at the outlet boundaries.

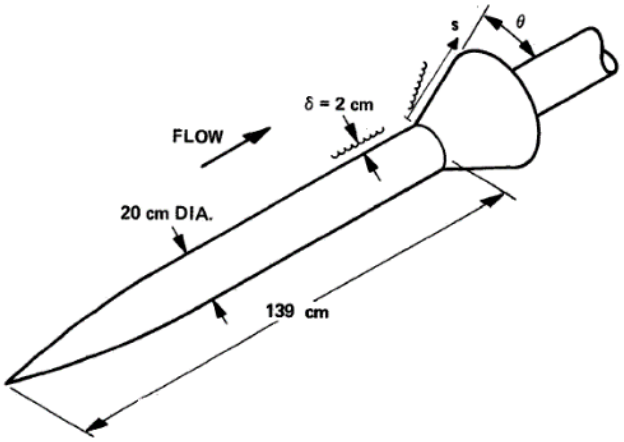

Fig. 1 The test model of the experiment of Kussoy and Horstman [23].

Table 1 Freestream boundary conditions for the Ma = 7.05 compression corner case

Ma_∞	Re_∞/m	T_∞, K	T_w, K	δ_0, cm	δ_0^*, cm
7.05	5,800,000	81.2	311	2.5	0.74

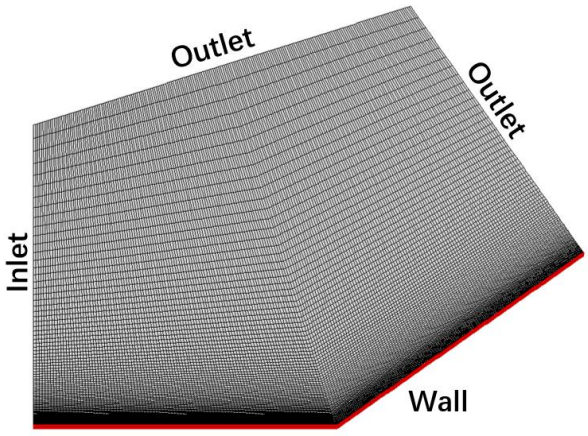

Fig. 2 Grid for the Ma = 7.05 compression corner case.

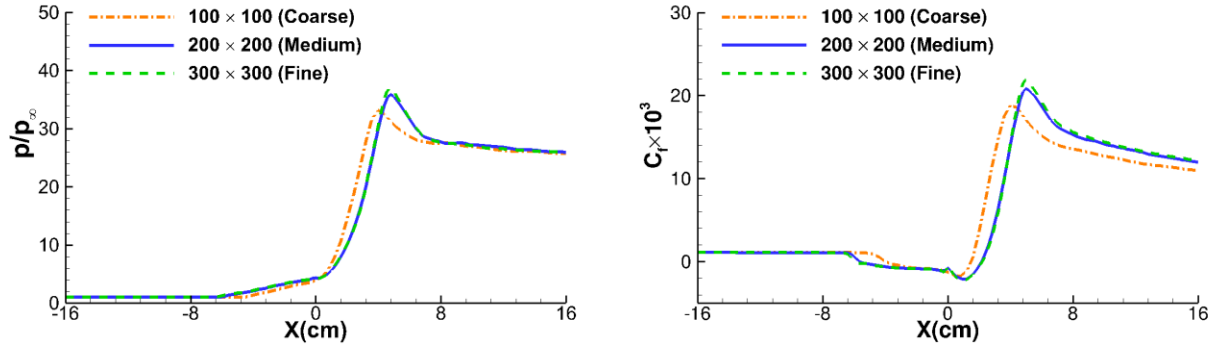

Fig. 3 Comparison of the predicted wall pressure (left) and skin friction coefficients (right) by three sets of grids for the Ma = 7.05 compression corner case at ramp angle of 35º.

The grid-independence test has been carried out by comparing the wall pressure and skin friction returned by three sets of grids for the case with ramp angle of 35º. The three grids used are 100×100 cells, 200×200 cells and 300×300 cells, where the values of y^+ at the first grid point off the wall has been kept at a value of less than 0.1. The comparison of the predicted results, shown in Fig. 3, shows that the coarse mesh returns a separation region obviously shorter than those of the other two grids. Little discrepancy exists between the medium mesh and fine mesh, which illustrates that the mesh of 200×200 cells is fine enough to return numerical results at a high level of grid independence so it will be used for all further calculations. Similar tests were also carried out for the other cases reported in this paper, to ensure that the results presented are grid independent.

The pressure fields predicted by the CLS model, at the flare angles of 20º and 35º, are shown in Fig. 4. An oblique shock wave is induced by the flare surface and, as the flare angle increases, the strength of the shock becomes greater and then a flow separation may occur around the corner. The separation induces another shock wave, which has an interaction with the boundary layer above the flare surface. The peak pressure in the interaction region goes from around 12 times the inflow pressure in the 20º case up to over 37 times in the 35º case.

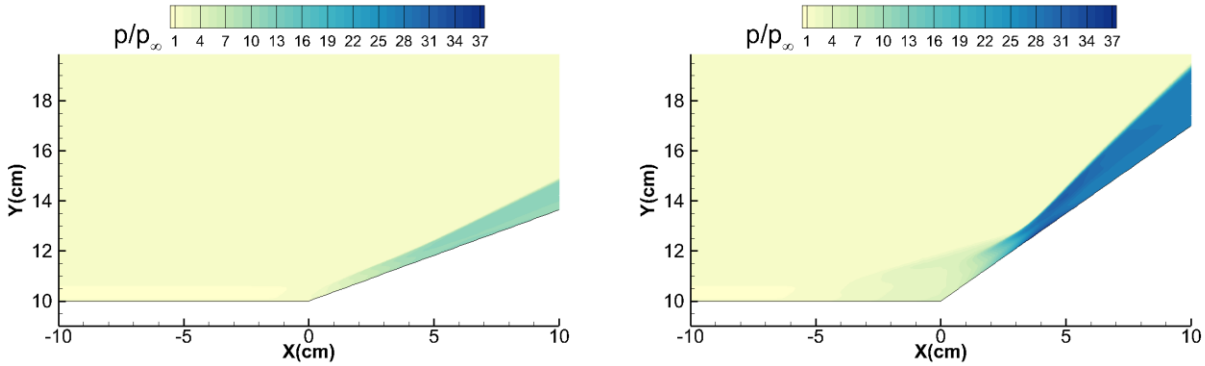

Fig. 4 Iso-lines of mean pressure for the Ma = 7.05 compression corner with flare angles of 20º(left) and 35º (right) predicted by the CLS model.

In Fig. 5, the local wall pressure and wall heat flux distributions at 20º flare, predicted by the three original models tested, are compared with the experimental data. For this attached flow case, these three models return basically identical pressure distribution, which agrees reasonably well with the data. The predictions of the wall heat flux also present only a weak sensitivity to the use of the original versions of the models, but all the predicted peak values are over 30% higher than that of the experimental data. The comparisons of the predicted wall pressure and wall heat flux at flare angle of 35º, given in Fig. 6, show that the LSY model tends to under-estimate the separation, while the SST model tends to over-estimate it, which results in either a shrunken or an over-extended pressure plateau upstream of the corner. The CLS model, however, agrees best with the measured pressure profile, with the peak of wall pressure better predicted as well as the pressure plateau induced by the separation. None of the three original models returns accurate predictions of the wall heat flux in the interaction region. The LSY model returns the least over-prediction among the three, but the peak value is 73% higher than that measured at the 35º flare angle. The over-estimation of the peak by the SST model is 85%, while the CLS model results in an even greater over-estimate, which is more than twice the experimental peak value.

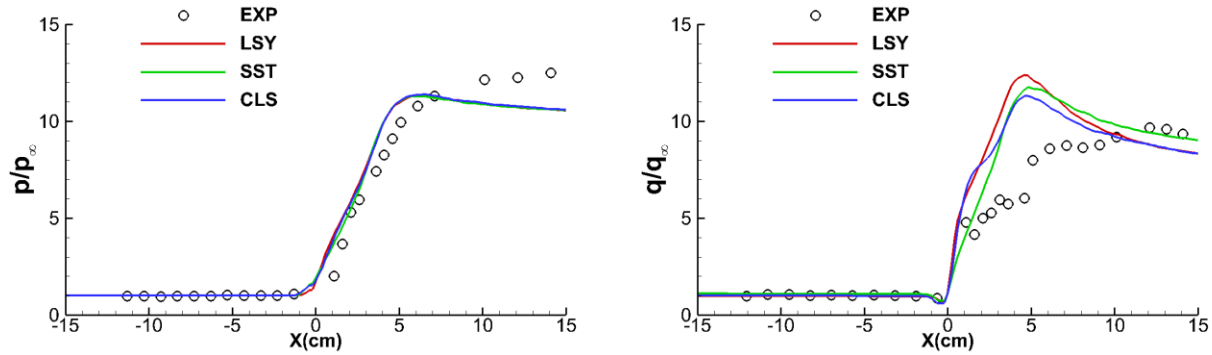

Fig. 5 Comparison of the predicted wall pressure (left) and heat flux (right) by the LSY, SST and CLS models with the experimental data for the Ma = 7.05 compression corner case with flare angle of 20º.

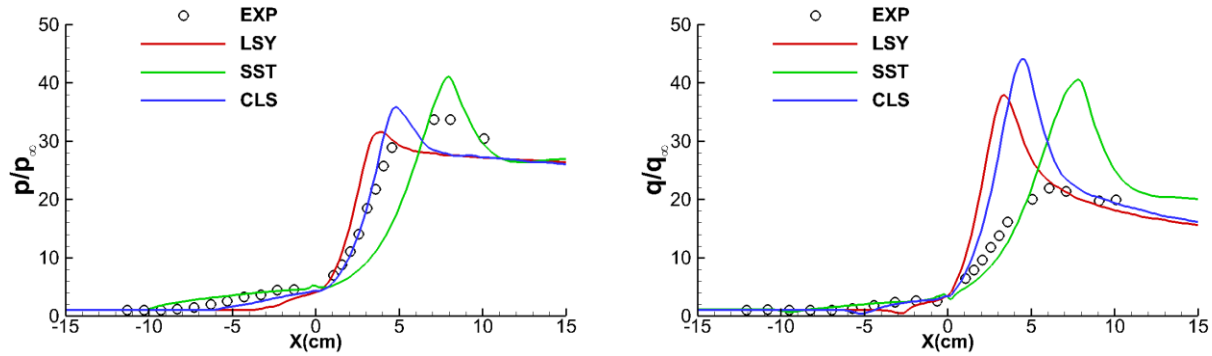

Fig. 6 Comparison of the predicted wall pressure (left) and heat flux (right) by the LSY, SST and CLS models with the experimental data for the Ma = 7.05 compression corner case with flare angle of 35º.

B. Coakley's[3] modification of Turbulent Length Scale

In the ε equation of the CLS model, a source term, the Yap correction term, is included, which tends to reduce the wall heat flux in a stagnation or reattachment region by controlling the turbulence length scale. However, from the numerical results, it seems that this correction is not enough to guarantee the wall heat flux to fit the experimental data in the reattachment region for flows with strong shock wave induced separation. Coakley, Horstman, Marvin, et al. [3] introduced an alternative form of length scale correction, which involves the use of an algebraic expression to limit the length scale employed in the model to that found in an equilibrium boundary layer. The correction used is given below:

$$l_c = \min(l_e, l) \tag{17}$$

where l_c is the turbulent length scale, which is taken to be the smaller of the equilibrium length scale, $l_e = 2.5y$, with y being the distance to the nearest wall, and the conventional length scale, $l = \frac{\sqrt{k^3}}{\tilde{\varepsilon}}$ for $\tilde{\varepsilon}$ based models or $l = \frac{\sqrt{k}}{\omega}$ for ω based models. This length scale limit was applied as a lower limit on the dissipation rate (or the equivalent in an omega formulation). The process followed, taking the $\tilde{\varepsilon}$ based models as an example, was that after solving the $\tilde{\varepsilon}$ equation, the dissipation rate $\tilde{\varepsilon}$ was then limited at each cell to be consistent with the value of $\tilde{\varepsilon} = \sqrt{k^3}/l_c$. Coakley, Horstman, Marvin, et al. [3] reported that the modification significantly improved the prediction of heat flux. Nevertheless, there is no physical evidence to suggest that the turbulent length scale has to be less than or equal to the equilibrium value in all flow cases.

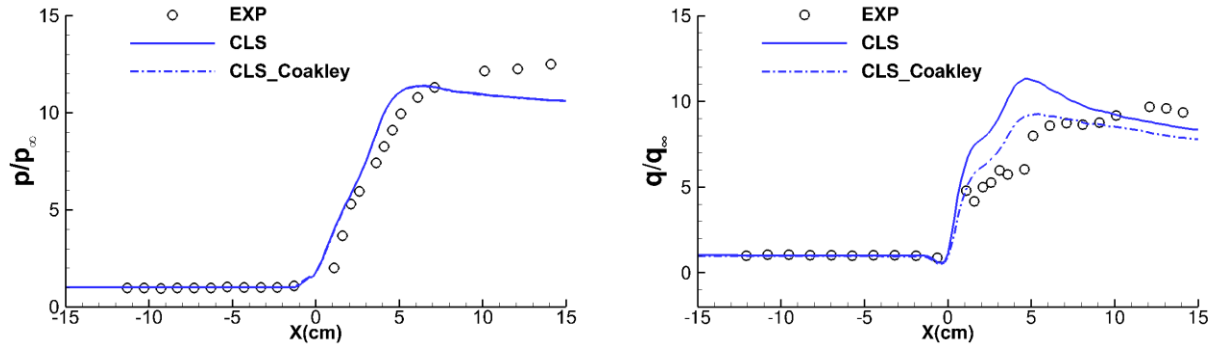

Fig. 7 Comparison of the predicted wall pressure (left) and heat flux (right) by the CLS and CLS_Coakley models with experimental data, for the case of Ma = 7.05 compression corner with flare angle of 20º.

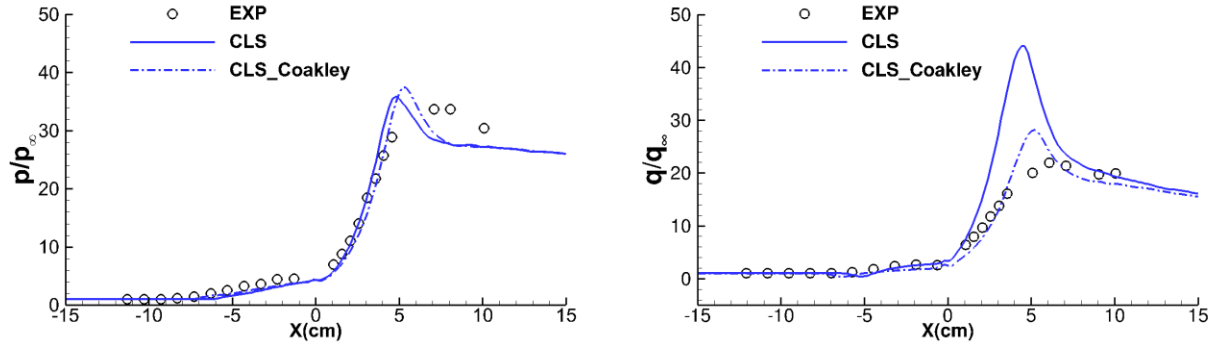

Fig. 8 Comparison of the predicted wall pressure (left) and heat flux (right) by the CLS and CLS_Coakley models with experimental data, for the case of Ma = 7.05 compression corner with flare angle of 35º.

The non-linear CLS model is selected here, as an example, to illustrate the effect of Coakley's modification. In Fig. 7 and Fig. 8, the resulting wall pressure and heat flux by the CLS model, with and without Coakley's modification,

at flare angles of 20º and 35º, are compared with the measured data. For the 20º case, the modification shows almost no impact on the pressure profile, while returning a lower peak of heat flux which is closer to the experimental value. In the case of 35º flare, the modified model returns a similar pressure profile as the original model does, except that the flow separation occurs slightly earlier. The peak of wall heat flux by the CLS_Coakley model, the CLS model with Coakley's modification, is now closer to that of the experimental data, with an overprediction of only around 30%. This comparison implies that by controlling the turbulent length scale, the wall heat flux does get reduced, whilst there is only a limited impact on the wall pressure distribution in this particular case. Thus, to control the growth of turbulence in the interaction region, alternative strategies could be to introduce another $\tilde{\varepsilon}$ source term to the transport equation of dissipation rate in the corresponding areas.

C. A New Turbulent Length Scale Correction

Although Coakley's modification does have some positive benefits in the SWBLI case above, it would also become active in supersonic, and even incompressible, flows. This is undesirable, since the CLS model has already been tested over a wide range of incompressible flows, showing generally good predictions. As will be seen in a later section, the introduction of Coakley's modification will lead to a significant reduction of wall friction in the interaction region in supersonic flows with SWBLI.

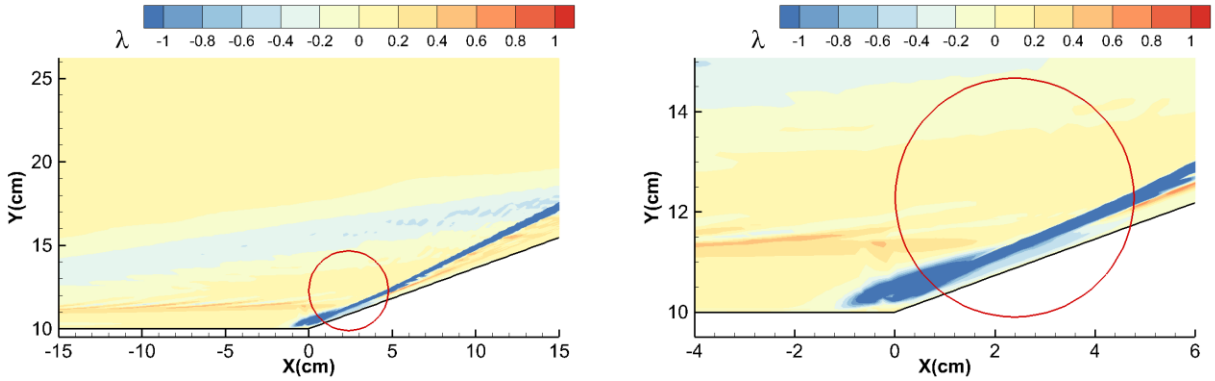

Fig. 9 Distribution of the normalised velocity divergence for the case of Ma = 7.05 compression corner with flare angle of 20º: major domain (left) and enlarged view (right).

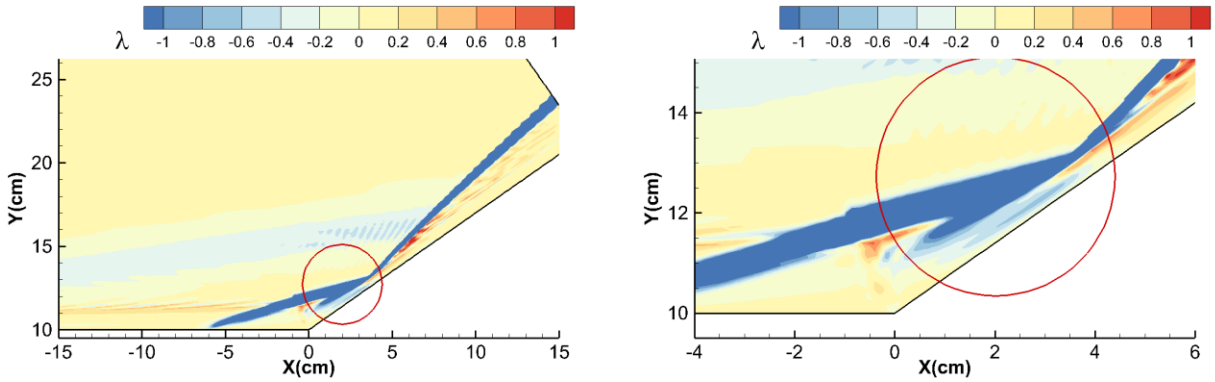

Fig. 10 Distribution of the normalised velocity divergence for the case of Ma = 7.05 compression corner with flare angle of 35º: major domain (left) and enlarged view (right)

Since the divergence of velocity for incompressible flow is zero, it can be used to distinguish the flow type. To explore how this might be applied, Figures 9 and 10 show the normalised velocity divergence

$$\lambda = \frac{k}{\tilde{\varepsilon}} \frac{\partial u_k}{\partial x_k} \tag{18}$$

ranging from -1 to 1, of the above compression corner flow at flare angles of 20º and 35º. In most of the flow field the divergence is zero or almost zero. In the regions corresponding to the shock waves, λ has a large negative value, indicated in dark blue. There is also a region between the ramp wall surface and the shock wave where λ takes significantly negative values (the regions in light blue within the red circled areas in Fig. 9 and Fig. 10). The negative value of velocity divergence in this region is mainly caused by flow compression, and the corresponding wall surface of this region is approximately the surface location where the wall heat flux is grossly overpredicted. Since the normalised divergence of velocity, λ, in this region, has a value from about -1 to 0, it was explored whether the value of λ could be used as a parameter to control a new source term of the dissipation rate equation, which, in turn, could also help to control the growth of turbulence. Therefore, a simple source term is proposed here to increase dissipation rate:

$$S_{\varepsilon cm} = H\lambda_l \frac{\tilde{\varepsilon}^2}{k} \tag{19}$$

where H is a constant number. Eq. (9) will not affect incompressible flows since $S_{\varepsilon cm} = 0$ when $\lambda = 0$, which satisfies a basic requirement of the modification. However, this modification would become active over the entire flow field as long as $\lambda \neq 0$, which does not align with the goal to only reduce the wall heat flux. So, in order to restrict this term to being mainly active only in the near-wall viscous region, where normally the turbulent shear stress is not dominant,

a function has been devised to switch off this modification when the strain rate or vorticity rise beyond a certain level. In the CLS model, the function of C_μ (see Eq. (11)) will return a value less than 0.09 when η becomes greater than 3.52 to control the turbulent eddy viscosity in the regions with high strain rate. Based on this, a function has been devised that deactivates the new source term when the C_μ function starts to influence the turbulent viscosity, of the form:

$$Y = tanh\big(2(\eta - 3)\big) - 1 \tag{20}$$

where η is the same as Eq. (12) and *tanh* is the hyperbolic tangent function. With the switch function of *Y*, which remains -2 for $\eta < 2$ and nearly zero for $\eta > 4$, the new source term becomes:

$$S_{\varepsilon cm} = HY\lambda_l \frac{\tilde{\varepsilon}^2}{k} \tag{21}$$

where *H* is a calibration constant, and $\lambda_l = \max\left(\frac{k}{\tilde{\varepsilon}}\frac{\partial u_k}{\partial x_k}, -0.5\right)$, which is designed to retain numerical stability.

The proposed source term would only become active in compressible flows and mainly be effective in the near wall or viscosity dominated regions. The next step is to tune the coefficient of *H* by comparing the numerical results with the experimental data to optimize the prediction of the wall heat flux. The value of the coefficient, *H*, was initially, set to 1, 2, 3 and 4 and the case of 35° used to examine the performance of this proposed modification.

The predicted wall pressure and heat flux, for values of the model constant *H* of 1, 2, 3, 4, are compared with the experimental data in Fig. 11, in which the CLS model with the $S_{\varepsilon cm}$ source term is noted as the CLS_M model. The peak values of wall pressure returned by the modified models are similar to each other and very close to that of the experiment. The profiles of wall pressure returned when *H* = 1 and 2 are almost identical and in close agreement with the measured values. The profile predicted when *H* = 3 shows a slightly larger separation than that of the two lower values of *H*, but still fits the experimental data very well. When *H* = 4, the separation is clearly over-estimated, indicating that the proposed source term is adding more dissipation than it should be. The wall heat flux predictions show greater differences in peak values than the corresponding computations of the wall pressure, suggesting that the proposed modification does have a stronger impact on the wall heat flux, as expected. The peak of wall heat flux when the model constant *H* is set to 4, is the closest to the experimental value, but it also develops a kink after the peak, which is not the case for the lower *H* values, nor is it seen in the experimental measurements. The reason for this kink may lie in the weak "numerical" unsteadiness, as can be seen from the periodic oscillation of the residuals of both the

mean and turbulent variables (shown in Fig. 12). The peak value is also reduced dramatically when H = 3, with an overprediction by about 20%, which is much lower than that of the original CLS model's 100%.

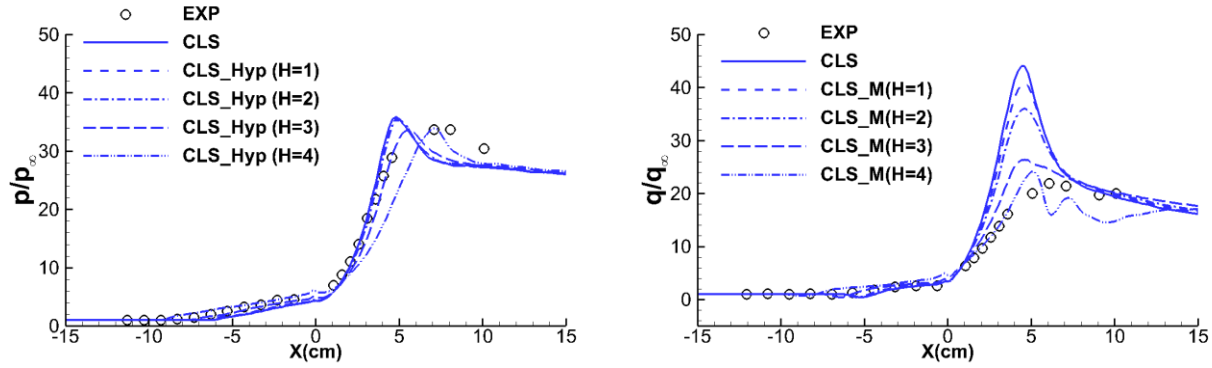

Fig. 11 The predicted wall pressure (left) and heat flux (right) by the CLS_M model with various values of the model constant "*H*", compared with that of the original CLS model and experiment, for the case of Ma = 7.05 compression corner with flare angle of 35º.

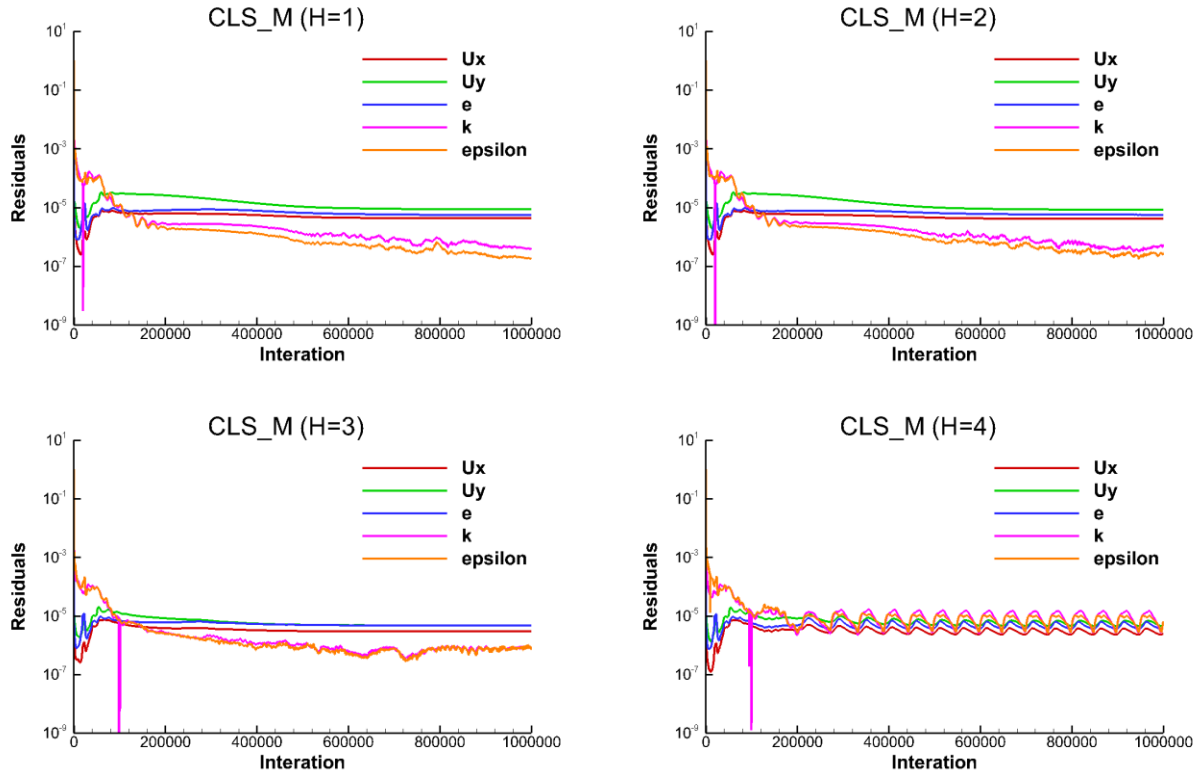

Fig. 12 Comparison of the residuals by the CLS_M model with various values of the model constant "*H*" for the case of Ma = 7.05 compression corner with flare angle of 35º.

The predictions resulting from a value of the model constant H of 3 show no kink in the wall heat flux profile and fit the measurements well in both the separation and reattachment regions. The results from H = 1 and 2 both show a

certain level of improvement compared to the original model, but not sufficient to overcome the overprediction. Therefore, the constant H is set to be 3 as the source term coefficient and the new source term can then be written as:

$$S_{new} = 3\lambda_l \frac{\tilde{\varepsilon}^2}{k}\left(tanh(2(\eta - 3)) - 1\right)\frac{\tilde{\varepsilon}^2}{k} \tag{22}$$

where $\lambda_l = \max\left(\frac{k}{\tilde{\varepsilon}}\frac{\partial u_k}{\partial x_k}, -0.5\right)$. With this new source term, the transport equation of dissipation rate could then be written as follows:

$$\frac{\partial \overline{\rho}\tilde{\varepsilon}}{\partial t} + U_j\frac{\partial \overline{\rho}\tilde{\varepsilon}}{\partial x_j} = C_{\varepsilon 1}f_1\frac{\tilde{\varepsilon}}{k}P_k - C_{\varepsilon 2}f_2\overline{\rho}\frac{\tilde{\varepsilon}^2}{k} + \frac{\partial}{\partial x_j}\left(\overline{\rho}\left(\nu + \frac{\nu_t}{\sigma_\varepsilon}\right)\frac{\partial \tilde{\varepsilon}}{\partial x_j}\right) + E + Y_c + S_{\varepsilon cm} \tag{23}$$

As the analysis and validation above has mainly focused on the 35º case, a fully separated flow, it is essential to examine the influence of the modification of Eq. (22) on a fully attached flow, such as the case of flare angle of 20º. The predicted and measured wall pressure and heat flux are compared in Fig. 13. As expected, the wall pressure profile returned by the CLS_M (H = 3) model shows little difference to that of the original model, which is in close agreement with the data. The wall heat flux, by contrast, is strongly influenced by this modification, and fits the experimental data much better than that of the original CLS model. The predicted peak value of the wall heat flux around the interaction region is almost at the same level as the measured value. There is a small kink close to the corner point in the prediction of the modified model. While there appears to be a similar kink in the experimental data , this may also be due to experimental scatter**.**

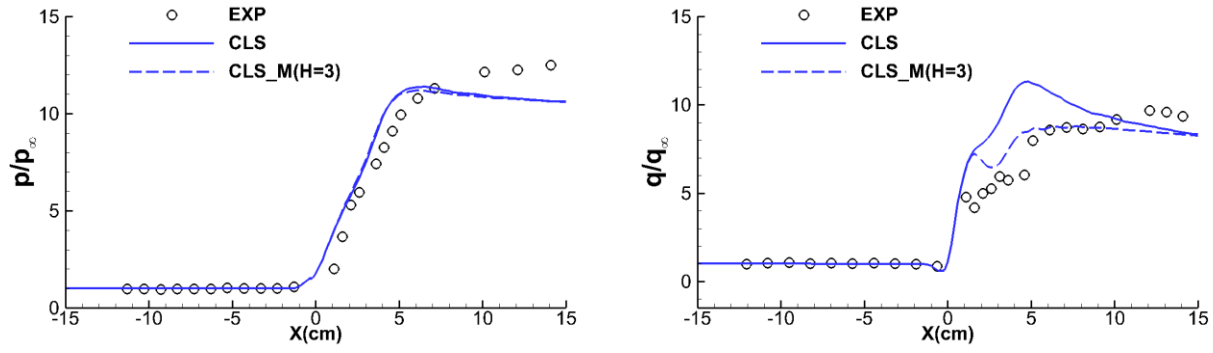

Fig. 13 The predicted wall pressure (left) and heat flux (right) by the CLS_M model with H = 3, compared with that of the original CLS model and experiment, for the case of Ma = 7.05 compression corner with flare angle of 20º.

So far, the modification of Eq. (22) has shown good promise in improving the prediction of wall heat flux for both attached and separated flows for this hypersonic compression corner flow, while retaining the already well-predicted

wall pressure. However, it is necessary to test the impact of this proposed modification to supersonic flows to ensure that it has no undesirable effect in them before testing other hypersonic cases. It is also worth examining the impact of such a term when used with other *k*-ε models, such as the linear LSY *k*-ε model.

D. Influence of Proposed Model Modification on Supersonic Flows and the linear LSY model

The Ma = 2.25 impinging shock case by Pirozzoli and Grasso [24] is considered here. The freestream condition, as well as the boundary layer information at the nominal impingement point, of the DNS calculation are listed in Table 2. A two-dimensional structured grid (160×130 cells), 5 cm × 2.5 cm shown in Fig. 14 (left), uniform in the streamwise direction and expanding exponentially in the direction normal to the wall, is used for the RANS simulations. Similar to the DNS, the part of the inlet boundary below the incoming shock wave is obtained from a separate flat plate boundary layer simulation which ensures the momentum thickness θ_0 of the boundary layer matches that of the DNS data at the impingement point. The use of the momentum thickness, as a reference to generate the inlet boundary conditions, is because information on displacement thickness was not available in the original paper. At the upper part of the inlet, the shock is artificially applied by specifying fixed values of the flow field satisfying the oblique shock wave relation with the shock wave angle of 33.2 degrees (the corresponding turn angle is about 8.1 degrees). Zero gradient boundary conditions for pressure and temperature, and no-slip boundary condition for velocity, are specified at the wall. Fig. 13 (right) is an overview of the predicted flow field by the CLS model, showing the Mach number contours of the computational domain**.**

Table 2 DNS flow conditions for the Ma = 2.25 impinging shock case

Ma_∞	Re_∞/m	T_∞, K	δ_0, cm	θ_0, cm
2.25	2,500,000	169.4	0.204	0.0147

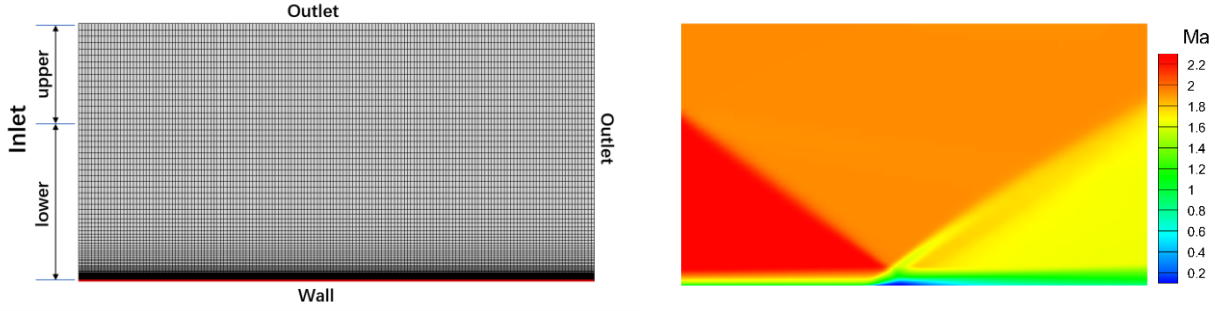

Fig. 14 Grid (left) and flow feature (right) of the Ma = 2.25 impinging shock case.

The predictions of wall pressure and skin friction by the CLS model incorporating the two different modifications, Coakley's modification and the new length scale correction, compared with the original CLS model and DNS data, are shown in Fig. 15. The introduction of these modifications results in very little change on the wall pressure distribution, with the modification of Eq. (22) giving an almost identical profile as the original CLS model and the CLS_Coakley model. The profiles of wall friction coefficient, however, exhibit a different pattern. The CLS_M model, the CLS model with the new length scale correction of Eq. (22), again returns a prediction very similar to that of the original CLS model, This confirms that the new source term is barely active in this case, as expected since the new source term was designed to have as little influence as possible on other flows except for hypersonic ones. All three models tested predict that flow separation starts earlier than what is observed in the experiment. The CLS_Coakley model also performs poorly in the prediction of the recovery region, where, compared to the CLS model, the separation length is over-estimated by over 30% and the wall friction coefficient is under-estimated by around 35% downstream of the reattachment point. The CLS and CLS_M models return recovery of separation closer to that indicated in the experimental data, in contrast to the poorer predictions of the linear LSY and SST models [17].

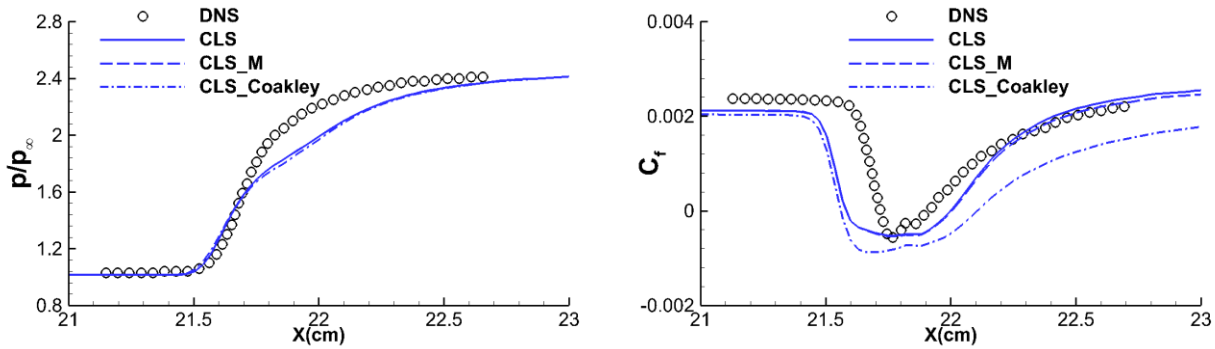

Fig. 15 Influence of the proposed modification of Eq. (22) and Coakley's modification to the CLS model on the predictions of wall pressure (left) and skin friction (right) for the Ma = 2.25 impinging shock case.

As the new source term of Eq. (22) has already shown a similar improvement as Coakley's modification did on the predictions of hypersonic flows with SWBLI, the much lower impact it has on supersonic SWBLI flows suggests that it could be more effective and more widely applied than the Coakley form. Thus, it is meaningful to test the performance of the new source term of Eq. (22) if it is added to the transport equation of the dissipation rate of the linear LSY model, as this is more widely used in many industrial simulations than the non-linear form. The hypersonic

compression corner flow with flare angles of 20º and 35º is used again to examine the performance of the LSY model with the newly proposed source term.

In Fig. 16 and Fig. 17, the wall pressure and heat flux predicted by the LSY model and LSY_M model, the LSY model with modification of Eq. (22), at corner angles of 20º and 35º are compared with the experimental data. In the lower angle case, the new source term has almost no influence on the predicted wall pressure distribution, but reduces the peak of wall heat flux significantly. The predicted peak of wall heat flux drops by about 30%, which is now in close agreement with the measured value. In the latter case, like the former one, only minor differences appear between the LSY and LSY_M models on the prediction of wall pressure, both of which present a shorter separation region than that of the experiment. The wall heat flux predicted by the LSY_M model, however, shows a strong improvement, where the overprediction of the peak is brought down from over 73% to about 22%, which is similar to what has been observed in the performance of the CLS_M model.

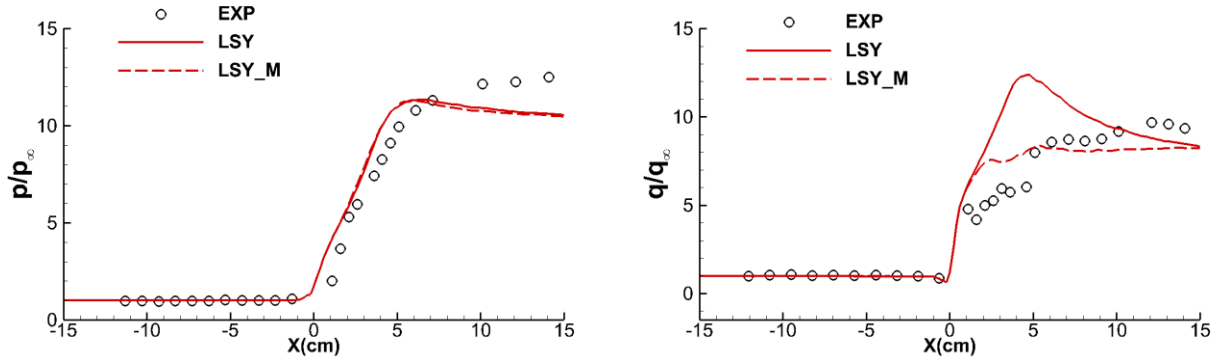

Fig. 16 Influence of the proposed modification of Eq. (22) to the LSY model on the predictions of wall pressure (left) and heat flux (right) for the case of Ma = 7.05 compression corner with flare angle of 20º.

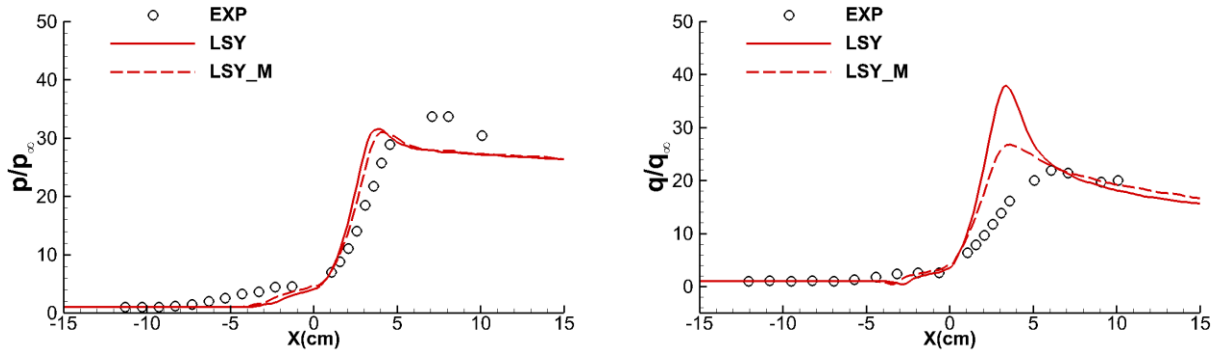

Fig. 17 Influence of the proposed modification of Eq. (22) to the LSY model on the predictions of wall pressure (left) and heat flux (right) for the case of Ma = 7.05 compression corner with flare angle of 35º.

E. Further Validation

The minor influence on the wall quantities in the supersonic cases and significant improvement on the predictions of wall heat flux presented by both the linear LSY and non-linear CLS models, as a result of the introduction of this proposed new source term of Eq. (22), demonstrate that this modification has a good potential to improve the predictions of wall heat flux in other hypersonic SWBLI flows. Therefore, to confirm this, more cases involving SWBLIs in the hypersonic regime have been tested in this section. The main goal of the comparisons here is focused on the predictions of the wall quantities, such as wall pressure and wall heat flux, over a range of Mach numbers and different types of hypersonic SWBLIs.

1. Ma = 7 Impinging Shock

The test models for the experiment of Kussoy and Horstman [25] are shown in Fig. 18, in which two different shock generators with turning angles of 7.5° and 15° were employed. The freestream conditions for the wind tunnel were total pressure = 34atm, total temperature = 695*K*, and Mach number = 7. Besides the nominal parameters for the wind tunnel, local flow conditions ahead of the interaction region were also reported for the two shock generators. The flow parameters for the shock generator angles of 7.5° and 15° , as well as the information of the undisturbed boundary layer ahead of the nominal impingement point (the leading edge of the shock generator is located at x = 0cm) are listed in Table 3, which are used to generate the inlet condition for the RANS simulations. Unlike the previous supersonic impinging shock case, the shock generator is included in the computational domain, shown in Fig. 19, and a structured grid, 400×300 cells, is used to discretize the flow field, in which the grid points in the streamwise direction are clustered at the leading edge of the shock generator and uniformly distributed in the interaction region and grow exponentially in the wall normal direction.

Table 3 Local flow conditions for the Ma = 7 impinging shock case

$\beta, °$	Ma_∞	p_∞, Pa	T_∞, K	$u_\infty, m/s$	T_w, K	x, cm	δ_0, cm	δ_0^*, cm
7.5	6.71	607	70.6	1129	300	42	3.3	1.237
15	6.86	607	67.8	1132	300	20	2.7	1.393

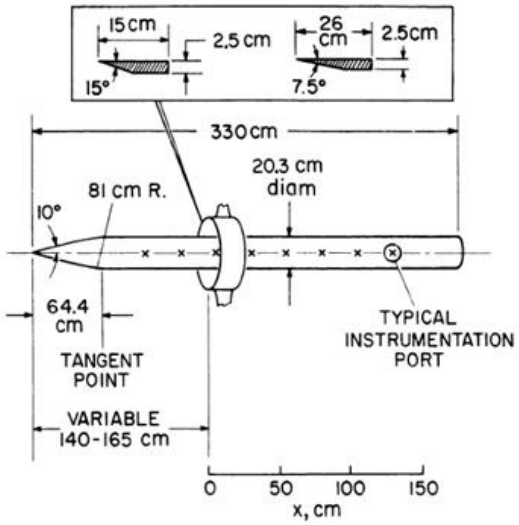

Fig. 18 Test model of the Ma = 7 impinging shock experiment (from Mikulla and Horstman [26]).

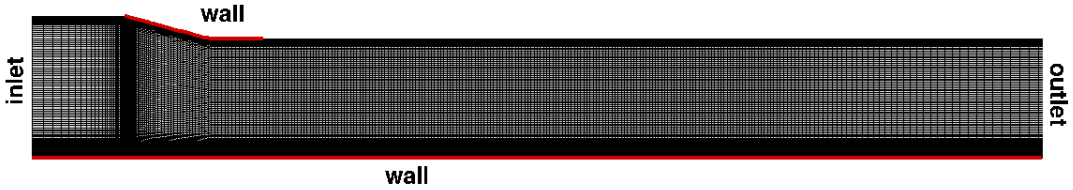

Fig. 19 Grid for the Mach = 7 impinging shock case.

The inlet boundary conditions are set to ensure the displacement thickness δ_0^* at the specified stations, 42cm and 20cm behind the leading edge of the shock generator for the 7.5° and 15° cases respectively, to match the measured values. The set inlet profiles are obtained from a separate calculation of undisturbed boundary layer flow on a cylinder under the conditions listed in Table 3. Zero gradient conditions are applied for all variables at the outlet boundary, and at the wall the no-slip condition is applied, with temperature fixed to the experimental value, and zero gradient for pressure.

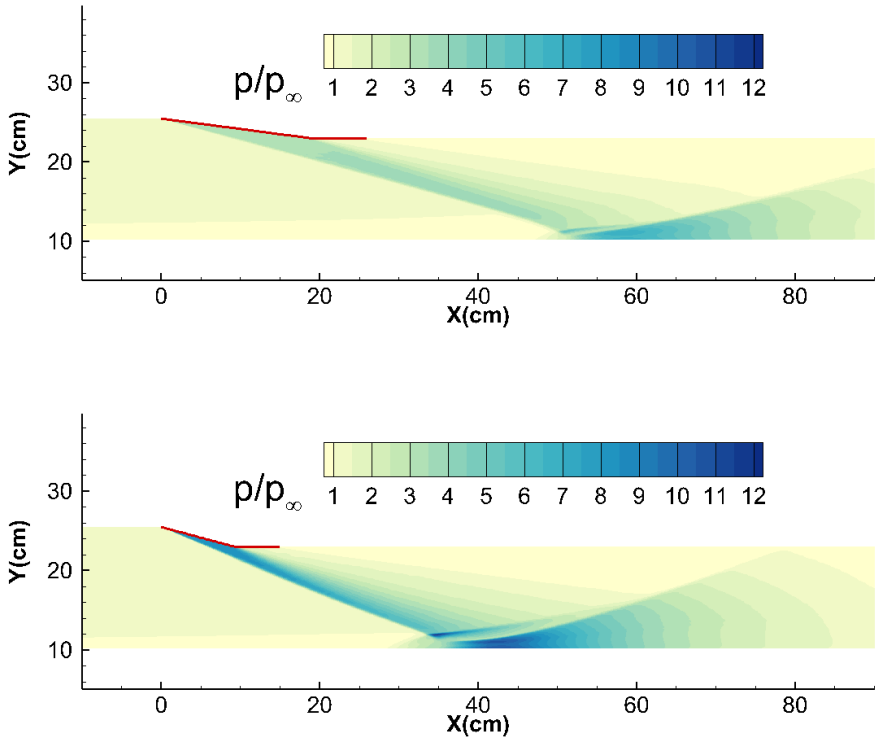

Fig. 20 Counters of mean pressure for the Ma = 7 impinging shock case with shock generator angles of 7.5º (top) and 15º (bottom) predicted by the CLS model.

The flow fields for the wedge angles of 7.5º and 15º, presented via the predicted pressure contours by the CLS model, are shown in Fig. 20. The increase of wedge angle from 7.5º to 15º results in a larger shock angle and greater pressure jump across the shock, which leads to a stronger adverse pressure gradient in the neighbourhood of the nominal impingement point. The boundary layer, therefore, can no longer remain attached and an obvious flow separation occurs. In Fig. 21, the streamlines predicted by the LSY, SST and CLS models, at the wedge angle of 15º, are compared with the experimental streamline contours. The predicted separation bubble by the CLS model fits the measured bubble better than the other two models. Although the separation length from the CLS model is slightly longer than that measured, both the separation point and the height of the bubble are in close agreement with the experimental data. The LSY model returns a much smaller separation bubble and later separation than that of the experiment, while the SST model over-estimates both the length and the height of the separation region, resulting in a much larger separation bubble.

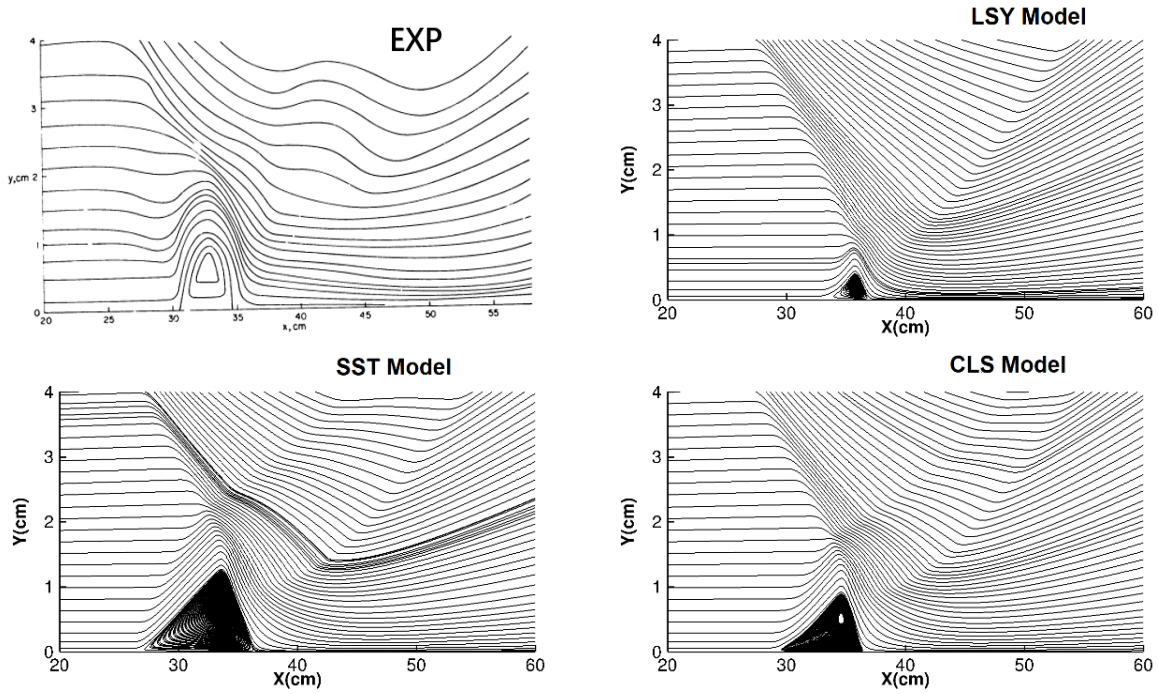

Fig. 21Streamlines for the Ma = 7 impinging shock case with shock generator angle of 15^o given by the experiment and the LSY, SST and CLS models (Note that the vertical scale has been stretched in these figures, in order to magnify the near wall separated flow structures).

Figure 22 compares the distributions of the local wall pressure and wall heat flux, predicted by the unmodified and the modified models at the wedge angle of 7.5^o. For the pressure, the LSY model returns a peak closer to that of the measurements than the other two unmodified models, but the pressure rise before the nominal impingement point is under-estimated. The SST and CLS models produce similar predictions of the peak value, which are about 10% lower than that of the data. The initial pressure rise predicted by the CLS model fits the data very well, while the SST model overpredicts it significantly. The pressure profiles downstream of the interaction region are well predicted by all these three models. The wall pressure predicted by the LSY_M and CLS_M models are almost identical to those from the unmodified models, which implies that the new source term, as expected, has little influence on the wall pressure distribution.

The peak of wall heat flux is overpredicted by all three unmodified models, but the SST model returns a closer prediction than the other two, overestimating the peak value by roughly 13%. The LSY model returns the greatest overprediction of the peak of the wall heat flux by a factor of 1.39, and the rise of wall heat flux before the nominal impingement point is not captured. The peak value predicted by the CLS model is about 23% higher than that of the experiment and the rise of wall heat flux upstream of the nominal impingement point is captured, but not as high as

in the measurements. By adding the new source term, a positive influence is induced to the predictions of the wall heat flux. Although the locations of the peak heat flux resulting from the use of the LSY_M and CLS_M models stay almost the same as the those of the unmodified models, a small distance away from the peak in the experiment, the actual peak values decrease by 11% and 12%, respectively, which now fit the measured values better.

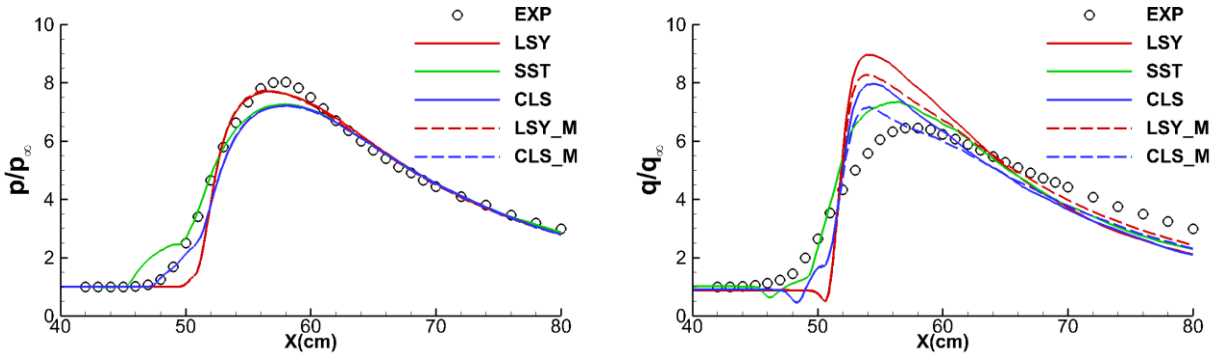

Fig. 22 Comparison of the predicted wall pressure (left) and heat flux (right) by the LSY, SST, CLS, LSY_M and CLS_M models with the experimental data for the Ma = 7 impinging shock case with shock generator angle of 7.5º.

The wall quantities at the wedge angle of 15º by the LSY, SST and CLS models, as well as the LSY_M and CLS_M models, are compared in Fig. 23. In contrast to the smaller angle case, the predicted peaks of wall pressure are all higher than that of the experimental data, with the SST and CLS models returning peak levels similar to each other, overpredicting the experimental data by around 20%. As demonstrated in the streamline comparisons, the LSY model underestimates the flow separation, only returning a very narrow plateau, which may be the reason for the 40%-overpredicted peak of the wall pressure. Although, compared to the experimental streamline contour, the SST model overpredicts the separation bubble, it returns a profile of the pressure plateau which is closer to that of the experimental data. The CLS model, on the other hand, returns a lower pressure plateau, although the size of the separation bubble produced by this model is the closest to that of the data. This phenomenon indicates that although some of the EVMs employed here can capture the sudden change in the stress, to a certain extent, they, even the non-linear model, could not provide enough of a response to the change, which results in the situation that an over-estimated bubble size by the SST model results in a pressure prediction closer to that of the measurements, than those of the other two models. Like in the 10º case, the wall pressure is not sensitive to the new source term, and the pressure profiles by the models with modification remain almost the same as their original ones.

The wall heat flux in the interaction region is again overestimated, but at a much more severe level than in the 10° case. The peak predicted by the LSY model is more than 1.7 times that of the experiment, while the SST and CLS models are better but still overpredict this value by around 35% and 43%, respectively. Downstream of the interaction region, the three unmodified models underpredict the wall heat flux by approximately 25 to 30 per cent. The new source term helps the LSY model bring down the significantly overpredicted peak from 70% higher than the experimentally measured value to around 47% overprediction. The CLS_M model returns the narrowest gap between the predicted and measured peaks of the wall heat flux among the four, with an overprediction of 18%, which is much less than the 43% overprediction by the CLS model. The modification also increases the predicted wall heat flux in the recovery region by about 10 to 15 per cent for both models, resulting in less of an underprediction of wall heat flux than the original models.

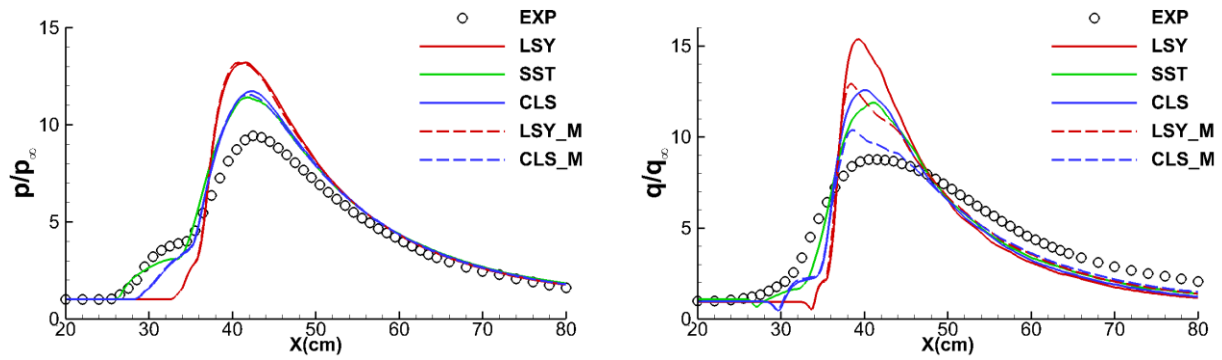

Fig. 23 Comparison of the predicted wall pressure (left) and heat flux (right) by the LSY, SST, CLS, LSY_M and CLS_M models with the experimental data for the Ma = 7 impinging shock case with shock generator angle of 15°

2. Ma = 9.22 Compression *Corner*

The test model of the experiments of Elfstrom [27] and Coleman and Stollery [28] is shown in Fig. 24, where the model consists of a flat plate with a sharp leading edge and an adjustable trailing-edge flap. The ramp angles considered here are 15° and 34°, with the former a fully attached flow and the latter a fully separated one. The nominal freestream conditions are given in Table 4, together with the reported boundary layer thickness measured at the end of the test surface with the flap kept horizontal (ramp angle = 0°). A two-dimensional structured grid, 300×200 cells, (see Fig. 25 (left)), uniform in the streamwise direction and expanding exponentially in the wall normal direction, was used for the RANS simulations. The flat plate and ramp surface are both 10cm long, which allows for the whole flow interaction region to be included. The profiles of flow variables imposed at the inlet boundary were obtained from a

separate flat plate boundary layer calculation to match the reported thickness at the end of the test model. No-slip conditions were applied at the wall, with temperature fixed to the experimental value and zero gradient for pressure. Zero gradient conditions were applied for all variables at the outlet boundaries. Fig. 25 (right) shows the flow feature, at the ramp angle of 34°, via the Mach number contours predicted by the CLS model.

Table 4 Freestream boundary conditions for the Ma = 9.22 compression corner case

Ma_∞	Re_∞/m	T_∞, K	T_w, K	δ_0, cm
9.22	47,000,000	64.5	295	0.72

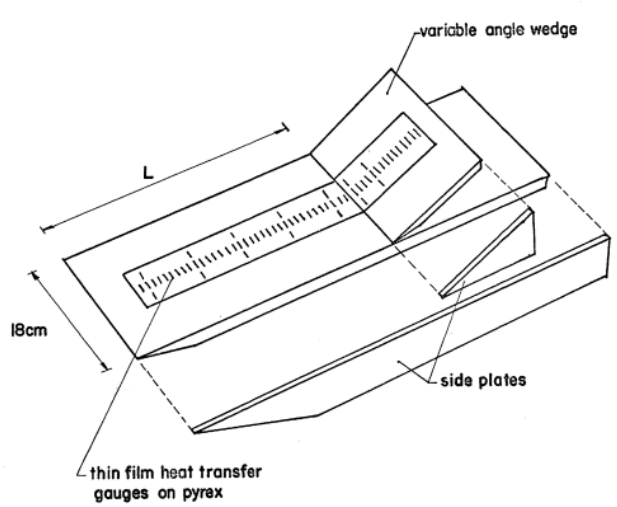

Fig. 24 The experiment model of the Ma = 9.22 compression corner case (from Coleman [29]).

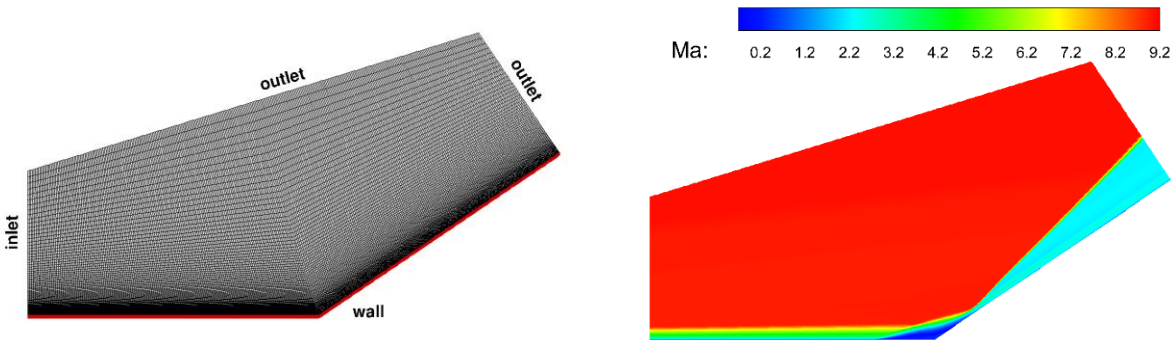

Fig. 25 Grid (left) and flow feature (right) of the Ma = 9.22 compression corner case.

The wall pressure and heat flux predicted, by the LSY, SST, CLS, LSY_M and CLS_M models, at corner angle of 15º, are compared with the experimental data in Fig. 26. The pressure profiles produced by the five models tested show very few differences among them, and the numerical results agree well with the data, the predicted peak wall pressure being only around 6.5% higher than that of the experiment. The three unmodified models all overestimate the peak of wall heat flux, with the CLS model deviating the least, by around 23% from the measurement, and the LSY model the most, about 40%. As expected, the new source term does reduce the wall heat flux in the interaction region, which brings the peak values predicted by both *k*-ε models to almost the same level as that of the experimental data.

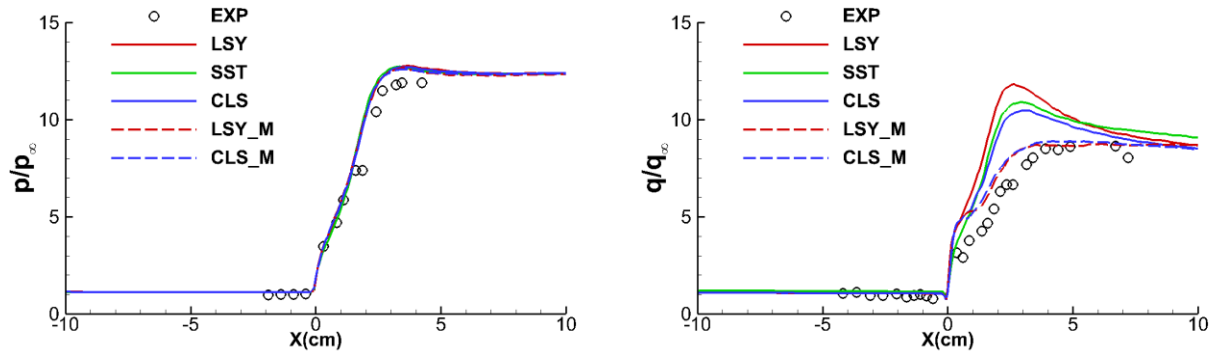

Fig. 26 Comparison of the predicted wall pressure and heat flux by the LSY, SST, CLS, LSY_M and CLS_M models with the experimental data for the Ma = 9.22 compression corner case with ramp angle of 15º.

The comparison between the wall pressure and heat flux profiles returned by the five models employed and those of the experiment, at corner angle of 34º, are shown in Fig. 27. The LSY model, again, tends to underestimate the flow separation, where the model fails to predict the pressure plateau and the sharp peak presented by the experimental data. The peak predicted by the LSY model is 16% lower than the measured value. The SST model, by contrast, returns a separation bubble that is much longer than that of the experiment and the peak of wall pressure is overpredicted by more than 36%. The CLS model returns better prediction of the wall pressure distribution than the two unmodified linear models, where the peak value and shape of the pressure variation are in close agreement with the data. The new source term added to the LSY model tends to hasten the separation. The shape of wall pressure profile predicted by the LSY_M model is now in closer agreement with the data, with the pressure rise captured and the peak of pressure only 5% lower than that measured. The introduction of the source term to the CLS model also results in the prediction

of a slightly earlier separation than with the CLS model itself, but the predicted wall pressure is still in close agreement with the data.

The wall heat flux in the interaction region is dramatically overestimated by all three unmodified turbulence models. The LSY model returns the closest peak to the data, but the overprediction is still over 45%. The peaks predicted by the SST and CLS models are about the same, which are twice the measured value. The LSY_M model presents a better prediction of the wall heat flux than its original form, where the resulting profile along the surface agrees better with the data and the peak is reduced by more than 25%. The use of the modification to the CLS model, again, reduces the predicted wall heat wall dramatically, and the peak value is now only 20% higher than that of the experiment.

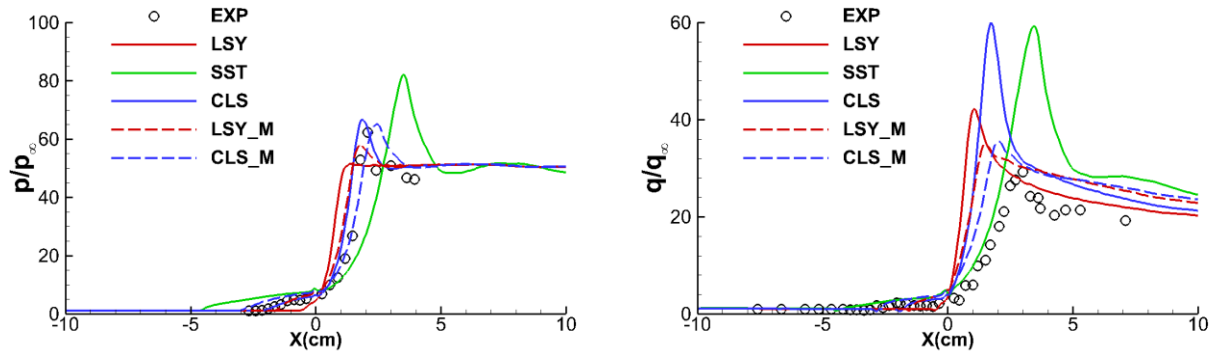

Fig. 27 Comparison of the predicted wall pressure and heat flux by the LSY, SST, CLS, LSY_M and CLS_M models with the experimental data for the Ma = 9.22 compression corner case with ramp angle of 34º

V. Conclusion

The performance of the non-linear CLS model has been evaluated by benchmark cases that involve shock wave boundary layer interactions in hypersonic flows. Comparisons have been also made against two linear eddy-viscosity turbulence models, namely the k-ε of Launder and Sharma, and k-ω SST model of Menter. A new turbulent length scale correction terms has been proposed with the aim of controlling the excessive turbulent length scale in the shock wave boundary layer interaction region at hypersonic speeds and causing as little influence as possible at lower Mach number flows. The original contributions of this research are: a) The systematic testing of the cubic non-linear k-ε model in the computation of hypersonic flows and the comparison of its predictions with those of the linear Launder-Sharma k-ε model and the k-ω SST model; b)The development of a length-scale correction term for hypersonic

conditions, which substantially improves the predictions of the non-linear k-ε model and also, just as importantly, of its linear counterpart. The main conclusions drawn are:

1) In general, the three original EVMs, the LSY, SST and CLS models, predict peaks of wall pressure broadly comparable to those of the experimental data, though in some cases the pressure rise caused by shock induced separation has been either underestimated or overestimated by the two linear models. The LSY model tends to underpredict the length of the separation bubble. By contrast, the SST model tends to overpredict the separation, especially in the two compression-corner cases. In most cases, the non-linear CLS model returned better predictions of the flow separation than the two linear models employed.
2) The peaks of wall heat flux in the interaction region were often overpredicted by the original versions of the three turbulence models tested, especially in cases with strong flow separation. For instance, in the Ma = 7.05 compression corner case with the 35º-flare, the overprediction of the peak wall heat flux was by more than 100% using the non-linear CLS model.
3) The turbulent length scale correction term proposed would naturally cause no impact on incompressible flow since it is zero in such cases, and numerical simulations of typical supersonic SWBLI cases showed that only minor influences might be induced on wall quantities in such flows.
4) The introduction of this new source term to the non-linear CLS model, the CLS_M model, had only a limited influence on the predictions of wall pressure and flow separation in hypersonic flows with SWBLIs, leaving the results in generally good agreement with measurements. This version of the model, CLS_M, however, has significantly reduced the severely overpredicted wall heat flux in the interaction region, and consequently the resulting distributions are in much closer agreement with the experimental data than the original model predictions.
5) It has also been demonstrated that this hypersonic flow length scale correction term can also be employed with the linear LSY model and provide significant improvements to the wall heat flux predictions, though the thermal predictions of the non-linear version, with the proposed term, are consistently closer to the measured data. This makes the effectiveness and universality of the new source term even greater.

Acknowledgments

Haoyuan Zhang gratefully acknowledges the financial support of the National Key Research and Development Plan of China through project No. 2019YFA0405202. This work is also supported partially by the National Natural Science Foundation of China (grant no. 12002361) and National Numerical Wind Tunnel Project of China.

References

[1] Dolling D. S., "Fifty Years of Shock-Wave/Boundary-Layer Interaction Research: What Next?," *AIAA Journal,* Vol. 39, No. 8, pp. 1517-1531, Aug 2001.
doi:10.2514/2.1476

[2] Roy C. J. and Blottner F. G., "Review and Assessment of Turbulence Models for Hypersonic Flows," *Progress in Aerospace Sciences,* Vol. 42, No. 7-8, pp. 469-530, Oct-Nov 2006.
doi:10.1016/j.paerosci.2006.12.002

[3] Coakley T. J., Horstman C. C., Marvin J. G., Viegas J. R., Bardina J. E., Huang P. G., and Kussoy M. I., "Turbulence Compressibility Corrections," NASA Technical Memorandum 108827, 1994.

[4] Rubesin M. W., "Extra Compressibility Terms for Favre-Averaged Two-Equation Models of Inhomogeneous Turbulent Flows," NASA Contractor Report June 1990.

[5] Vuong S. T. and Coakley T. J., "Modeling of Turbulence for Hypersonic Flows with and without Separation," *25th AIAA Aerospace Sciences Meeting*, Reno,NV, 1987.

[6] Lindblad I. A. A., Wallin S., Johansson A. V., Friedrich R., Krogmann P., Schiilein E., Courty J.-C., Ravachol M., and Giordano D., "A Prediction Method for High Speed Turbulent Separated Flows with Experimental Verification," *29th AIAA, Fluid Dynamics Conference, Fluid Dynamics and Co-located Conferences*, 1998.

[7] Huang P. G., Bradshaw P., and Coakley T. J., "Turbulence Models for Compressible Boundary-Layers," *AIAA Journal,* Vol. 32, No. 4, pp. 735-740, Apr 1994.
doi:10.2514/3.12046

[8] Huang P. G., Coleman G. N., and Bradshaw P., "Compressible Turbulent Channel Flows: Dns Results and Modelling," *Journal of Fluid Mechanics,* Vol. 305, pp. 185-218, Dec 25 1995.
doi:Doi 10.1017/S0022112095004599

[9] Duan L., Beekman I., and Martin M. P., "Direct Numerical Simulation of Hypersonic Turbulent Boundary Layers. Part 2. Effect of Wall Temperature," *Journal of Fluid Mechanics,* Vol. 655, pp. 419-445, Jul 25 2010.
doi:10.1017/S0022112010000959

[10] Xiao X., Hassan H. A., Edwards J. R., and Gaffney R. L., "Role of Turbulent Prandtl Numbers on Heat Flux at Hypersonic Mach Numbers," *AIAA Journal,* Vol. 45, No. 4, pp. 806-813, Apr 2007.
doi:10.2514/1.2144

[11] Jordan C., Buss G., Edwards J. R., and Stefanski D. L., "Rans and Les Simulation of a Mach 7 Axisymmetric Flare Interaction," *AIAA Scitech 2020 Forum*, 2020, p. 1331.

[12] Jordan C., Edwards J. R., and Stefanski D. L., "Evaluation of Rans Closure Models Using Les Datasets for Hypersonic Shock Boundary Layer Interactions," *AIAA Scitech 2021 Forum*, 2021, p. 1666.

[13] Craft T. J., Iacovides H., and Yoon J. H., "Progress in the Use of Non-Linear Two-Equation Models in the Computation of Convective Heat-Transfer in Impinging and Separated Flows," *Flow Turbulence and Combustion,* Vol. 63, No. 1-4, pp. 59-80, 2000.
doi:10.1023/A:1009973923473

[14] Launder B. E. and Sharma B. I., "Application of the Energy-Dissipation Model of Turbulence to the Calculation of Flow near a Spinning Disc," *Letters in Heat and Mass Transfer,* Vol. 1, pp. 131-138, 1974.
doi:10.1016/0094-4548(74)90150-7

[15] Yap C. R., "Turbulent Heat and Momentum Transfer in Recirculating and Impinging Flows," Ph.D Thesis, Faculty of Technology, University of Manchester, 1987.

[16] Menter F. R., Kuntz M., and Langtry R., "Ten Years of Industrial Experience with the Sst Turbulence Model," *Turbulence, heat and mass transfer,* Vol. 4, No. 1, pp. 625-632, 2003.

[17] Zhang H., Craft T. J., and Iacovides H., "The Formulation of the Rans Equations for Supersonic and Hypersonic Turbulent Flows," *The Aeronautical Journal,* Vol. 125, No. 1285, pp. 525-555, 2021.
doi:10.1017/aer.2020.93

[18] Kim K. H., Kim C., and Rho O. H., "Methods for the Accurate Computations of Hypersonic Flows - I. Ausmpw+ Scheme," *Journal of Computational Physics,* Vol. 174, No. 1, pp. 38-80, Nov 20 2001.
doi:10.1006/jcph.2001.6873

[19] Van Albada G., Van Leer B., and Roberts Jr W., "A Comparative Study of Computational Methods in Cosmic Gas Dynamics," *Astronomy and Astrophysics,* Vol. 108, pp. 76-84, 1982.
doi:10.1007/978-3-642-60543-7_6

[20] Greenshields C. J., Weller H. G., Gasparini L., and Reese J. M., "Implementation of Semi-Discrete, Non-Staggered Central Schemes in a Colocated, Polyhedral, Finite Volume Framework, for High-Speed Viscous Flows," *International Journal for Numerical Methods in Fluids,* Vol. 63, No. 1, pp. 1-21, May 10 2010.
doi:10.1002/fld.2069

[21] Zhang H. Y., "Turbulence Modelling for Aerodynamic Heating in Hypersonic Flows," PhD Dissertation, Department of Mechanical, Aerospace and Civil Engineering, University of Manchester, Manchester, England, 2021.

[22] Craft T. J., Launder B. E., and Suga K., "Development and Application of a Cubic Eddy-Viscosity Model of Turbulence," *International Journal of Heat and Fluid Flow*, Vol. 17, No. 2, pp. 108-115, Apr 1996.
doi:10.1016/0142-727x(95)00079-6

[23] Kussoy M. I. and Horstman C. C., "Documentation of Two- and Three Dimensional Hypersonic Shock Wave/Turbulent Boundary Layer Interaction Flows.," NASA Technical Memorandum 101075, 1989.

[24] Pirozzoli S. and Grasso F., "Direct Numerical Simulation of Impinging Shock Wave/Turbulent Boundary Layer Interaction at M=2.25," *Physics of Fluids*, Vol. 18, No. 6, Jun 2006.
doi:10.1063/1.2216989

[25] Kussoy M. I. and Horstman C. C., "An Experimental Documentation of a Hypersonic Shock-Wave Turbulent Boundary Layer Interaction Flow—with and without Separation," NASA TECHNICAL MEMORANDUM 1975, vol. NASA TM X-62,412.

[26] Mikulla V. and Horstman C. C., "Turbulence Measurements in Hypersonic Shock-Wave Boundary-Layer Interaction Flows," *AIAA Journal*, Vol. 14, No. 5, pp. 568-575, 1976.
doi:10.2514/3.7127

[27] Elfstrom G. M., "Turbulent Hypersonic Flow at a Wedge-Compression Corner," *Journal of Fluid Mechanics*, Vol. 53, No. May9, pp. 113-127, 1972.
doi:10.1017/S0022112072000060

[28] Coleman G. T. and Stollery J. L., "Heat-Transfer from Hypersonic Turbulent-Flow at a Wedge Compression Corner," *Journal of Fluid Mechanics*, Vol. 56, No. Dec28, pp. 741-752, 1972.
doi:10.1017/S0022112072002630

[29] Coleman G. T., "Hypersonic Turbulent Boundary Layer Studies," PhD Dissertation, Department of Aeronautics, Imperial College of Science and Technology, 1973.